Proceedings of the 7th European VLBI Network Symposium
Bachiller, R. Colomer, F., Desmurs, J.F., de Vicente, P. (eds.)
October 12th-15th 2004, Toledo, Spain

The Water Vapour Radiometer at Effelsberg

A. L. Roy, U. Teuber and R. Keller

Max-Planck-Institut für Radioastronomie, Auf dem Hügel 69, 53121 Bonn, Germany

Abstract. We have installed a scanning 18 GHz to 26 GHz water vapour radiometer on the focus cabin of the Effelsberg 100 m telescope for tropospheric phase, delay and opacity correction during high-frequency VLBI observations. It is based on the design by Tahmoush & Rogers (2000) but with noise injection for calibration, weather-proof housing, and temperature stabilization. The radiometer is delivering data into an archive since July 2003, from which they are available for download. The data will be delivered automatically to PIs of EVN experiments in a calibration table attached by the EVN calibration pipeline. This paper describes the radiometer and its performance.

1. The Effelsberg Water Vapour Radiometer

Some views of the water vapour radiometer (WVR) are shown in Fig. 1. The radiometer is located on top of the prime focus cabin looking skyward along the optical axis. The basic parameters are given in Table 1, and the project status is maintained at `http://www.mpifr-bonn.mpg.de/staff/aroy/wvr.html` .

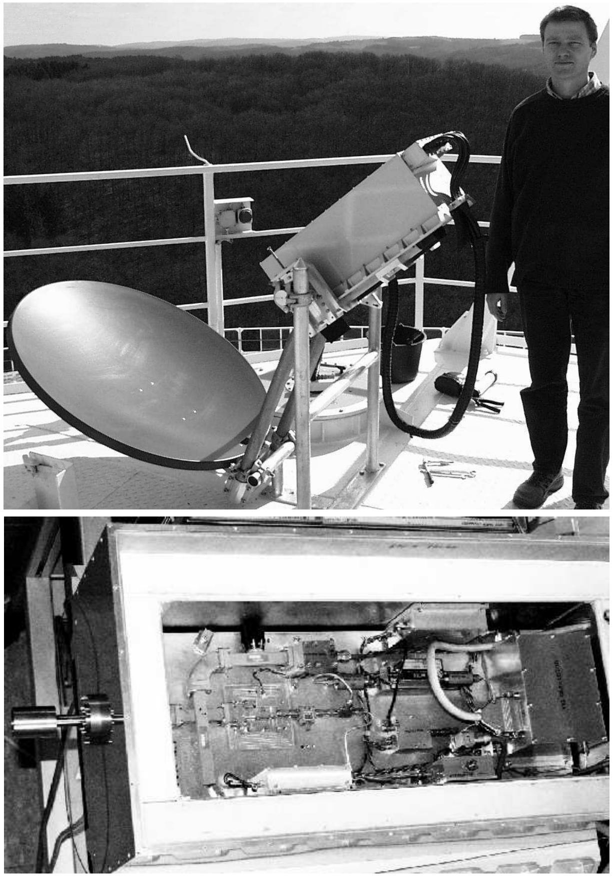

Fig. 1. Top: View of the radiometer on top of the primary-focus cabin at Effelsberg. Bottom: Front end opened, showing waveguide components mounted on a temperature-stabilized plate in an insulated box.

Table 1. Basic parameters of the Effelsberg WVR

Frequency	18.3 GHz to 26.0 GHz
Channels	25
Bandwidth	900 MHz
T_{receiver}	200 K
Physical temperature	25 °C
Temperature stabilization	Peltier cooler
Thermal noise	61 mK in 0.025 s per spectrum (= 0.27 mm path length noise, assuming 4.5 mm K^{-1})
Absolute accuracy	~ 1 % of T_{sys} (= 9 mm path length systematic offset assuming 4.5 mm K^{-1})
Gain stability	2.7×10^{-4} over 400 s
Sweep Time	5 s
Beamwidth	1.3° for best main-beam overlap
Gain calibration	noise injection or measured T_{internal}
Monitor and control	ethernet on optical fibre
Integrated water vapour retrieval	by fitting theoretical line profile to measured spectrum and frequency-squared term for cloud component and a constant term for calibration errors. Upgrade to *Atmospheric Transmission at Microwaves* (Pardo et al.) is pending.

2. How it Works

The block schematic of the front end is shown in Fig. 2. The low-noise amplifier covers the 18 GHz to 26 GHz band with a receiver temperature of 200 K to 230 K. A yttrium-iron garnet (YIG) local oscillator is steered between 18.8 GHz and 25.7 GHz and mixes the RF signal to baseband using a double-sideband conversion. The signal is filtered to 450 MHz bandwidth (equivalent to 900 MHz at RF), is detected by a square-law detector, and is sampled by a commercial ethernet data acquisition system (EDAS). All RF components are mounted on a temperature-stabilized plate in an insulated weather-proof enclosure. The online software uses a socket connection to the EDAS unit over the intranet to issue commands to steer the lo-

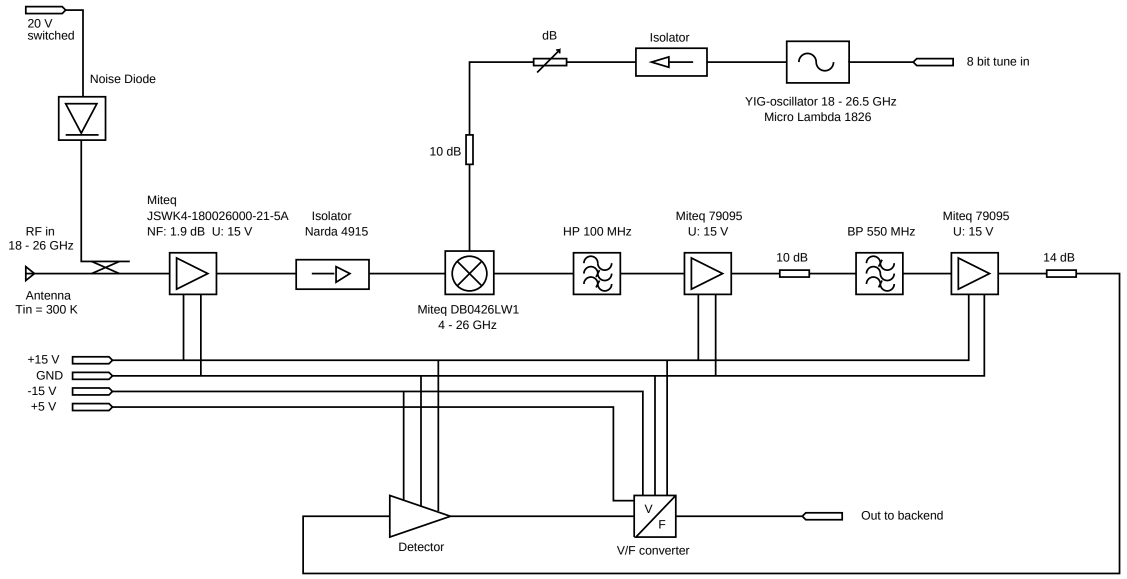

Fig. 2. Block schematic of the front end

cal oscillator, point the radiometer, fire the noise diode, read back the detector output level, and read back monitor points.

Each spectrum acquired is calibrated immediately by the online software by dividing by the gain (measured previously against a hot load and the cold sky, using a skydip to measure the sky temperature), then subtracting the frequency-dependent receiver temperature and the elevation-and-frequency-dependent spillover temperature. The spectrum is then fit by a three-component model consisting of a frequency-squared term which models black-body emission from the ground and from liquid water in clouds, a Van Vleck-Weisskopf line profile which models the water vapour emission, and a constant term which models residual calibration errors. The brightness temperature of the water vapour line is related to excess path length due to refractivity of the atmosphere by a scale factor, which, for surface air temperature of 273 K and surface air pressure of 990 hPa is $\sim$ 4.9 mm K^{-1}. This approach was developed by Tahmoush & Rogers (2000). The extraction of path length from radiometer measurements has since been incorporated into the Atmospheric Transmission at Microwaves (ATM) software package by J. Pardo (2003, private communication) and we will soon use this in place of the three-component fit. The calibrated sky spectra and atmospheric path lengths are written to an SQL database along with a time-stamp, from where they can be examined and downloaded through a web interface, which is being developed.

3. Performance Requirements

3.1. Tropospheric Phase Fluctuation Correction

Coherence on a baseline after atmospheric phase correction should be (somewhat arbitrarily) at least 0.9. When observing at 3.4 mm, this requires an rms path length noise after atmospheric phase correction of 0.18 mm, using the Ruze (1966) formula. The noise comes from four sources (thermal noise, gain fluctuations, beam mismatch and calibration noise) at each end of the baseline, so each noise source should contribute at most $1/\sqrt{8}$ of that, or 0.064 mm, corresponding to 14 mK using a nominal scale of 4.5 mm K^{-1}. This stability should be achieved on the time-scale of a single VLBI scan which is conventionally 400 s at present. This can be translated into a requirement for the gain stability as follows. Gain fluctuations multiply the typical zenith water-line brightness of 45 K, (derived from the median atmospheric conditions measured by radiosonde at Essen, Germany [Crewell, private communication]) and the resulting error should not exceed 14 mK, so the gain stability should be 14 mK /45 K = 3.1×10^{-4}. Example time series of antenna temperature on the sky and on absorber are shown in (Fig. 3, top and middle), showing that the radiometer easily detects fluctuations in the atmospheric emission. The Allan variance of the radiometer (Fig. 3, bottom) was measured on the ambient absorber and showed stability of 2.7×10^{-4} on a 400 s time-scale, better than required.

3.2. Phase Referencing

VLBI phase referencing rarely achieves a dynamic range better than 20:1, due to errors in the assumed station positions and zenith tropospheric delay. The EVN station position estimates have recently been refined, yielding better phase referencing performance (Charlot et al. 2002). The tropospheric model remains the largest source of error at high frequency.

We can derive the precision required for the measurement of total atmospheric delay with the radiometer, starting with a requirement that the calibrated phase on the target source should be in error by not more than a radian. Assuming an observation at 45° elevation, an elevation difference of 3° between calibrator and target, an observing wavelength of 1.3 cm, then a one-radian error in the transferred phase corresponds to a 22 mm error in the total zenith tropospheric delay. The majority of this error likely comes from the changing wet component,

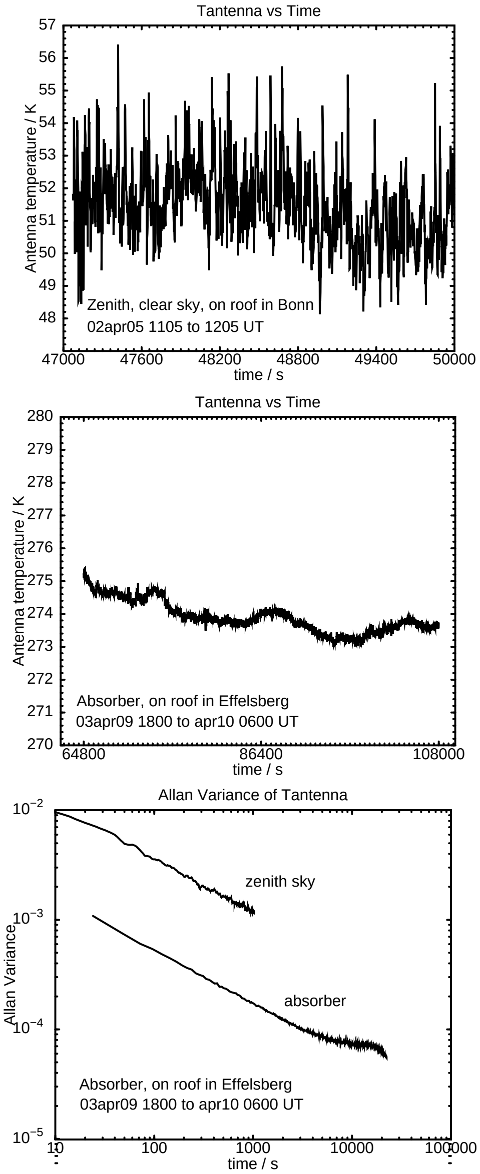

Fig. 3. Top left: time series of T_{antenna} at zenith on clear blue sky for 1 h shows fluctuations mostly due to atmospheric water vapour. Integration time was 0.3 s per point. Top right: Time series of T_{antenna} on an ambient-temperature absorber for 12 h shows much smaller fluctuations, due to gain and absorber temperature changes. Integration time was 0.025 s per point. Bottom: Allan variance of the time series.

which can be measured by the radiometer. Measured values of zenith wet delay at Effelsberg during 2003 and 2004 were typically in the range 70 mm to 300 mm. The worst-case zenith wet delay of 300 mm, requires 7 % absolute calibration accuracy.

Absolute calibration uses a hot load and cold sky, for which the uncertainty is typically 1 % due to uncertainty in the absorber temperature, sky temperature measurement, and efficiency of coupling radiation into the radiometer. Absolute measurements are sensitive also to errors in the atmospheric model used for retrieval of the water vapour content from the sky spectrum, which might have 3 % uncertainty (eg Delgado et al. 2003).

Thus, the absolute calibration of the radiometer is probably better than required for phase referencing at 22 GHz.

4. Sky Survey

All-sky panoramas in Effelsberg and Bonn (Fig. 4) were made to determine the horizon limits and to survey the interference environment. They were made in 1° steps, by scanning in elevation at each azimuth and measuring a 30-point spectrum at each position. The RFI in Bonn was, unsurprisingly, prohibitively strong, but in Effelsberg the spectrum was clean and allowed good measurement of atmospheric water vapour emission.

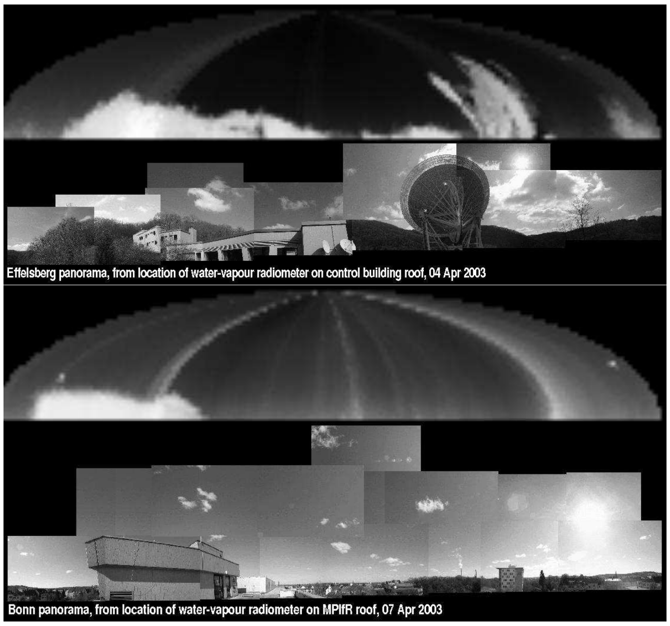

Fig. 4. 360° panoramas in Effelsberg (top pair) and in Bonn (bottom pair) made by the water-vapour radiometer and the optical view for comparison. One frequency channel was selected from which to render the images (22.2 GHz at Effelsberg and 20.5 GHz in Bonn). North is in the middle, the radiometer images are to the same scale, and the optical images are approximately to the same scale. The sky in Effelsberg showed streaks due to changing atmospheric water vapour column caused by weather changes during the four-day measurement period. The Effelsberg 100 m telescope appeared streaked because the telescope moved during the measurement. The panorama in Bonn is dominated by streaks caused by transmitters around the city, making the sky generally brighter than in Effelsberg (both images are calibrated and presented with the same greyscale range). A gradient in the sky brightness is visible nevertheless, due to the longer path length through the atmosphere at low elevation. The white dot above the building near the left edge of the image is the sun and that near the right hand edge of the image is a geostationary satellite.

5. The Measured Water Line

Two examples are shown in Fig. 5 of line profiles and the corresponding sky conditions under which they were measured. The spectrum measured by the radiometer is shown in the left half of each example and the simultaneous view from a camera looking along the axis of the radiometer is shown in the right frame. The water line is prominent and, as the cloud thickened, both the line and the baseline levels rose, until under the heaviest storm conditions the baseline swamped the line and the measurements were then not reliable.

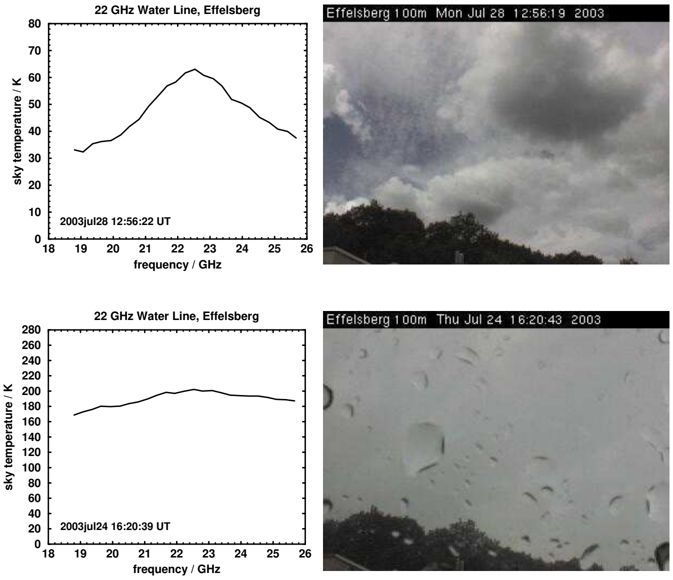

Fig. 5. Examples of water line spectra (left) and the corresponding sky conditions (right) measured on 2003 Jul 24 and 28 from the control-building roof in Effelsberg, looking towards azimuth = 330°, elevation = 30°. At the top, one sees fair-weather cumulus and below is during an intense storm with rain.

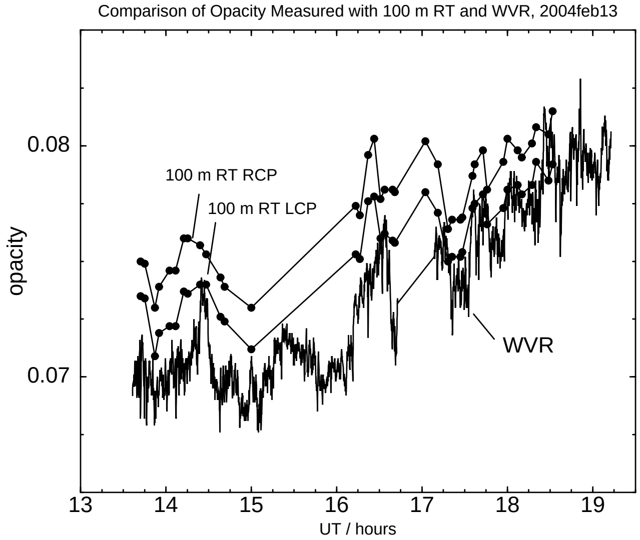

Fig. 6. Opacity vs time at 22.2 GHz estimated with the Effelsberg 100 m radio telescope using T_{sys} vs elevation (filled circles) towards sources at various elevations compared with opacity measured by the WVR (continuous line), showing good agreement. Atmospheric opacity is not polarization dependent, so the difference between opacities determined in the left and right circular polarization channels indicates the level of internal errors in the Effelsberg opacity measurement. The WVR measurements agree with the Effelsberg measurements within the uncertainties.

6. Data Validation Tests

We validated the opacity measurements by observing with Effelsberg 100 m at 22 GHz, performing cross scans on sources at various elevations while the WVR measured opacities at a fixed position on the sky. Opacities were derived from the Effelsberg data using the elevation dependence of T_{sys}, following an established procedure (A. Kraus, private communication). We compared the two time series of opacities after mapping them to the zenith with a $1/\sin(el)$ mapping function (Fig. 6) and found agreement within the uncertainties.

Validation of zenith delay data in phase referencing experiments and of phase correction data in 13 mm and 3 mm VLBI experiments has yet to be completed.

7. Data Delivery to the PI

For EVN experiments, the calibration pipeline at JIVE will automatically download WVR data, convert sky spectra to path-length and opacity at the observing frequency using ATM, and attach a calibration table in which this measured atmosphere replaces the atmosphere used during correlation. The PI can then look at the data with and without the corrections by choosing to apply the appropriate calibration table.

The WVR archive can also be examined and downloaded through a web interface, offering download formats suitable for AIPS for interferometry, CLASS for single-dish application, a format (yet to be specified) for geodesy, and XML and ascii for those wishing to delve deeper. Follow the links from `http://www.mpifr-bonn.mpg.de/staff/aroy/wvr.html`. The same web pages will later offer a real-time view of conditions and trends for making dynamic scheduling decisions.

8. Conclusion

A new water-vapour radiometer has been installed at Effelsberg and data are available for opacity correction and, after validation tests are complete, for phase correction. The radiometer measured in parallel with 86 GHz VLBI in April 2004 and detailed comparison between the WVR data and the VLBI phases is in progress.

Acknowledgements. We thank Alessandra Bertarini for providing her expertise with IDL, without which the sky survey images would not have been made.

This research was supported by the European Commission's I3 Programme "RADIONET", under contract No. 505818.

References

Charlot, P., Campbell, R.M., Alef, W., et al. in Proc 6th European VLBI Network Symposium, Eds E. Ros, R. W. Porcas, A. P. Lobanov, & J. A. Zensus (Max-Planck-Institut für Radioastronomie, Bonn), 9

Delgado, G., Rantankyrö, F.T., Pérez Beaupuits, J.P., & Nyman, L.Å, 2003, ALMA Memo 451

Pardo, J.R., Cernicharo, J., & Serabyn, E. 2001, IEEE Transactions on Antennas and Propagation, Vol 49, No. 12, 1683

Ruze, J. 1966, Proc IEEE, 54, 633

Tahmoush, D.A. & Rogers A.E.E. 2000, Radio Science, 35 (5), 1241